Holographic spectral functions in metallic AdS/CFT

JHEP09(2009)032

(http://iopscience.iop.org/1126-6708/2009/09/032)

Published by IOP Publishing for SISSA

Received: *June 9, 2009*
Revised: *August 19, 2009*
Accepted: *August 27, 2009*
Published: *September 4, 2009*

Holographic spectral functions in metallic AdS/CFT

Javier Mas, Jonathan P. Shock and Javier Tarrío

Departamento de Física de Partículas, Universidade de Santiago de Compostela, Instituto Galego de Física de Altas Enerxías (IGFAE), E-15782 Santiago de Compostela, Spain

E-mail: jamas@fpaxp1.usc.es, shock@fpaxp1.usc.es, tarrio@fpaxp1.usc.es

Abstract: We study the holographic $D3/D7$ setup dual to $\mathcal{N}=4$ supersymmetric Yang-Mills with quenched fundamental matter. We extend the previous analyses of conductivity and photoproduction to the case where there is a finite electric field. Due to the electric field a special region in the $D7$-brane geometry, labelled the singular shell, appears generically, and the computation of correlators involves a careful study of the indicial exponents both at this singular region and at the horizon. We show that there is a unique choice consistent with the known expression for the electrical conductivity found by Karch and O'Bannon [1]. We explore the parameter space spanned by the quark mass, the baryon density and the electric field. We find a region where the conductivity and photoproduction change rapidly and trace this behavior to competing effects which manifest themselves as a rapid change in behavior in the probe brane embeddings, related to possible thermodynamic instabilities.

Keywords: Gauge-gravity correspondence, D-branes, AdS-CFT Correspondence

ArXiv ePrint: 0904.3902

doi:10.1088/1126-6708/2009/09/032

JHEP09(2009)032

Contents

JHEP09(2009)032

1 Introduction

Since its original formulation, the AdS/CFT correspondence has been applied to an extremely diverse range of phenomena. Only recently, the applications to non-relativistic systems [2] and superconductivity [3, 4] have been elucidated and a large number of papers on these subjects continue to be published. One of the most recent applications of the correspondence has been to study gauge theories in the presence of electric and magnetic fields [1, 5–12], a useful way to explore the properties of many physical systems.

In this paper we are interested in the study of strongly coupled plasmas, in particular the Dp/Dq brane intersections holographically dual to Yang-Mills theory with fundamental hypermultiplets [14, 15]. We will use the benchmark $D3/D7$ system in order to study the properties of such plasmas, generalising wherever possible to the Dp/Dq intersection.

One of the first additions to the most basic AdS/QGP (Anti-de-Sitter/Quark Gluon Plasma) calculations was the introduction of a finite charge density [16, 17]. This corresponds to studying a Dq-brane probe in a black Dp-brane background (a geometry with

an AdS boundary and a black hole at the centre) with the time component of a world-volume gauge field on the Dq-brane turned on. One of the most striking consequences of the addition of finite charge density was the disappearance of the, so called, "Minkowski embeddings" [17]. These Minkowski embeddings correspond to Dq-branes which wrap vanishing cycles which end away from the black hole horizon. These solutions are characterised by a discrete spectrum of excitations corresponding to infinitely long-lived bound states. However, no matter how small the quark density introduced, the bulk gauge field flux lines need somewhere to end, and the only option is the horizon, removing the possibility of having Minkowski embeddings. An immediate consequence of this is that the introduction of heavy flavors with finite charge density leads to flavor probe brane embeddings which, as they run in from the AdS boundary into the IR, are flat all the way down to some small region where they develop a long spike which eventually hits the horizon. All embeddings in this setting then take the form of "Black Hole", or "Schwarzschild embeddings". In more physical terms, this means that with any finite quark density, all mesons are unstable and the spectral function becomes continuous. It also means that the "fundamental phase transition" between stable and unstable mesons disappears.

In this setting, the magnitude of the charge density can be used as a control parameter in which the smooth, continuous spectral functions tend, in the vanishing charge density limit, to those of the stable phase with its signature discrete spectral function. In this way one can approach the stable meson phase arbitrarily close. In the limit where the spectral function takes the form of sharp peaks one can study the dispersion relation of the modes in the plasma by tracking the peak positions in the frequency plane as a function of their momenta. This was performed for transverse excitations in [18] and for the more involved longitudinal ones in [19]. For the transverse case subluminal asymptotic velocities were observed, while in the second, some evidence for superluminal propagation was obtained. This second, rather more exotic behavior is currently under study by looking at the fully fledged quasinormal mode calculation [20].

The next step in exploring these kinds of systems is the introduction of electric and/or magnetic fields within the holographic setups at zero and finite temperature. In [1, 7–9, 21] the phase structure of these systems was studied in detail, while the spectrum of excitations was also looked at in a certain subsector of the phase diagram. In the present study we will be interested in extending this work to the rest of the phase diagram in the case of the electric field, where the behavior is more complicated than in the magnetic case. For similar studies in the Sakai Sugimoto model see [11–13].

In the electric case, for small enough ratios of the quark mass to the electric field strength, the probe Dq-brane becomes unstable, the signature of this instability being a region on the brane's worldvolume where the lagrangian becomes complex [1, 9]. The solution to this pathology is the introduction of a current in the direction of the electric field. Though this removes the pathology, the remnant of this is a submanifold of the Dq-brane worldvolume where the lagrangian density vanishes on-shell. This submanifold is known in the literature variously as the "singular shell" [8] and the "ergosphere" [10] (due to its interpretation in the T-dualised geometry). It turns out that for any given electric field strength, there is a unique current which will cure the pathology. The ratio

JHEP09(2009)032

of the current to the electric field then provides a definition of the D.C. conductivity, as would be computed via a simple Ohm's law experiment.

Although the singular shell cures the problem of having an ill-defined action, it does introduce new complications. In particular in order to compute the spectral function for excitations on top of classical embeddings which pass through the singular shell, the boundary conditions for the excitation, which are non-trivial, must be understood. In this paper we solve this problem, thereby allowing us to calculate more physical quantities in this interesting setup.

A check that we have the correct boundary conditions will be to compare the D.C. conductivity calculated from the macroscopic setup [1] to that calculated using the Kubo relation, which involves the excitations on top of the classical brane embedding. Once the correct boundary conditions have been found we will be able to calculate the spectral function for light-like momenta and thereby study the photoproduction rate for the plasma in the presence of an electric field.

The parameter space that we are interested in is spanned by the magnitude of the electric field, the quark mass and the charge density, and in the course of studying the spectral function we will discover a region of particular interest in it. In this region there is a very rapid change in behavior of the spectral function, going quickly from smooth oscillations to sharp spikes as we traverse this region of the tunable parameters. The change in behavior can be seen in several distinct physical quantities, including the conductivity, the susceptibility and the photoproduction rate. The behavior can be traced back to a rapid change in behaviour of the embedding solutions which affects all subsequent quantities. We show that for different regions in the parameter space this rapid change corresponds to a crossover or a first order phase transition.

The outline of the paper is as follows: In section 2 we introduce our holographic setup. Wherever possible we work within the framework of the general Dp/Dq flavor brane intersection. In this context we derive the constants of motion and the conductivity as given in [1] .

In section 3 we turn to the specific case of the $D3/D7$ intersection and illustrate the various types of brane behavior present by a series of plots. We then examine the change in the profiles upon a continuous variation of the electric field and the quark mass, as described above, and find the region where there is a rapid change. Sometimes, but not always, this abrupt change is the signal of a first order phase transition. We carefully . We also study the effect of this transition on the chiral condensate, charge susceptibility, conductivity and diffusion which can be derived directly from the background embedding solutions.

In section 4 we move on to the computation of correlators. We do this for transverse fluctuations only, propagating in the direction of the background electric field. We show that this is enough to compute the conductivity using the Kubo relation. This can be done analytically for general Dp/Dq systems and we find perfect agreement with the expression in [1].

In section 5, in order to calculate the correlation functions away from the hydrodynamic limit we again specialize to the case of the $D3/D7$ setup. We study the transverse

JHEP09(2009)032

correlator at zero momentum for different values of the electric field and see that the change in the embedding behavior has a large effect on the spectral function. From the same function evaluated on the light-cone we obtain the photoproduction rate. On integrating this magnitude to obtain the total luminosity we find a dramatic increase in the total number of emitted photons upon traversing the crossover/phase transition region.

We finally summarize our results and comment on possible extensions to the current work.

2 Holographic setup: background solutions

In this section we summarize the framework used to study the embedding of N_f probe Dq-branes in the background of a stack of $N_c \gg N_f$ coincident Dp-branes. This has been studied in many contexts in the literature, and a review of such investigations can be found in [22]. We will start here by detailing the generic Dp/Dq intersection and later specialise to the $D3/D7$ system.

On a stack of coincident Dq-probe branes there is a natural U(N_f) global symmetry whose abelian center can be identified with a baryonic U(1) symmetry. The dynamics of the brane embeddings and of the U(1) gauge field is dictated by the probe Dq-brane DBI action

$$\mathcal{S}_{\rm DBI} = -N_f T_{D_q} \int_{D_q} \mathrm{d}x^{q+1} e^{-\phi} \sqrt{-\det(g_{ab} + 2\pi\alpha' F_{ab})}, \tag{2.1}$$

where $T_{D_q} = 1/((2\pi\sqrt{\alpha'})^q g_s \sqrt{\alpha'})$ is the Dq-brane tension, g_s the string coupling, α' the inverse string tension and g_{ab} the pullback metric from the 10-dimensional background. Here we will not deal with isospin degrees of freedom, hence any possible non-abelian effects are ignored. The background in which we wish to place these probe branes is the near-horizon limit of a stack of non-extremal Dp-branes

$$ds_{10}^2 = G_{AB}\mathrm{d}X^A\mathrm{d}X^B = H^{-\frac{1}{2}}\left(-f(r)\mathrm{d}x_0^2 + \mathrm{d}\vec{x}_p^2\right) + H^{\frac{1}{2}}\left(\frac{\mathrm{d}r^2}{f(r)} + r^2\mathrm{d}\Omega_{8-p}^2\right), \tag{2.2a}$$

$$e^{\phi} = H^{(3-p)/4}, \qquad C_{01\cdots p} = H^{-1}, \tag{2.2b}$$

$$H(r) = \left(\frac{R}{r}\right)^{7-p}, \qquad f(r) = 1 - \left(\frac{r_h}{r}\right)^{7-p}, \tag{2.2c}$$

and the Hawking temperature is given by

$$T = \frac{7-p}{4\pi R}\left(\frac{r_h}{R}\right)^{\frac{5-p}{2}}. \tag{2.3}$$

The probe branes wrap an n-sphere in the directions transverse to the Dp-branes, so we write

$$\mathrm{d}\Omega_{8-p} = \mathrm{d}\theta^2 + \sin^2\theta\mathrm{d}\Omega_n^2 + \cos^2\theta\mathrm{d}\Omega_{7-p-n}^2, \tag{2.4}$$

setting the classical Dq-brane embedding by a functional dependence[1] $\cos\theta \equiv \psi(r)$. The Dq-brane pullback metric is written as

$$\mathrm{d}s^2 = g_{ab}\mathrm{d}x^a\mathrm{d}x^b = g_{00}(r)\mathrm{d}{x_0}^2 + g_{ii}(r)\mathrm{d}\vec{x}_p^2 + g_{rr}(r)\mathrm{d}r^2 + g_{\Omega\Omega}(r)\mathrm{d}\Omega_n^2, \tag{2.5}$$

[1] this is possible by exploiting an $O(8-p-n)$ symmetry.

JHEP09(2009)032

where the components of the induced metric g_{ab} will coincide with the components of the background 10-dimensional metric G_{ab} except for the radial term, given by

$$g_{rr} = G_{rr} + G_{\theta\theta}(\psi)\psi'(r)^2 = \frac{H^{1/2}}{f(r)}\left(1 + r^2 f(r)\frac{\psi'^2}{1-\psi^2}\right) . \tag{2.6}$$

All of the following analytic results will hold for any AdS black hole metric whose time component goes to zero linearly at the horizon, independent of the coordinate system chosen. All physical results will also be independent of redefinitions of the radial coordinate. Here we will consider both finite charge density and a finite electric field directed along one of the spatial directions of the Minkowski space, say x^p. The holographic ansatz for the world-volume gauge field that takes these two contributions into account is

$$A = A_0(r)\mathrm{d}x^0 + \left(E_p x^0 + A_p(r)\right)\mathrm{d}x^p . \tag{2.7}$$

$A_0(r)$ and $A_p(r)$ will be normalizable solutions to the equations of motion, and their leading terms in an expansion around the asymptotic AdS boundary correspond to the vacuum expectation values (*vevs*) of current densities $J^0(x)$ and $J^p(x)$ respectively. The non-normalizable piece, $E_p x^0$, is dual to the source of the current, namely the electric field itself.

For compactness we will define a new matrix given by $\gamma_{ab} = g_{ab} + (2\pi\alpha')\,F_{ab}$. The only non-diagonal components of this matrix, γ_{ij}, are found when i, j take values in $i, j \in \{0, p, r\}$. We also define $\gamma^{ab} = \gamma_{ab}^{-1}$ and $\gamma \equiv \det \gamma_{ab}$.

The DBI action for our Dp/Dq system is given by equation (2.1), and can be expressed as[2]

$$\mathcal{S}_{\mathrm{DBI}} = -N_f T_{D_q} \int \mathrm{d}^{p+1}x\, \mathrm{d}r\, \mathrm{d}\Omega_n\, e^{-\phi}\sqrt{-g_{ii}^{p-1} g_{\Omega\Omega}^n\, W} , \tag{2.8}$$

where the coefficients g_{ab} are those of equation (2.5) and

$$W(r) = \det \gamma_{ij} = g_{rr}\left(g_{00}g_{ii} + (2\pi\alpha')^2 {E_p}^2\right) + (2\pi\alpha')^2\left(g_{ii}A_0'^2 + g_{00}A_p'^2\right) .$$

There are two conserved quantities, n_q and j_p, related to the charge density and the electric current respectively and defined by

$$\frac{\delta\mathcal{S}_{\mathrm{DBI}}}{\delta A_0'} = \frac{n_q}{\Omega_n} , \qquad\qquad \frac{\delta\mathcal{S}_{\mathrm{DBI}}}{\delta A_p'} = \frac{j_p}{\Omega_n} ,$$

where Ω_n is the volume of the unit n-sphere. The gauge field components can then be solved for as follows

$$A_0' = -\frac{n_q}{\sqrt{g_{ii}}}\sqrt{-\frac{g_{rr}g_{00}\left(g_{00}g_{ii} + {E_p}^2(2\pi\alpha')^2\right)}{\mathcal{N}^2 e^{-2\phi} g_{00} g_{ii}^p g_{\Omega\Omega}^n + (2\pi\alpha')^2\left(g_{00}n_q^2 + g_{ii}j_p^2\right)}} , \tag{2.9a}$$

$$A_p' = \frac{j_p}{n_q}\frac{g_{ii}}{g_{00}}A_0' , \tag{2.9b}$$

where $\mathcal{N} = N_f T_{D_q}\Omega_n(2\pi\alpha')^2$. As $g_{00} < 0$ (provided we are outside any possible horizons in the geometry), there is a radius $r_\star(E_p)$ such that $g_{00}g_{ii}(r_\star) + {E_p}^2(2\pi\alpha')^2 = 0$. This

[2] we will consider only fluctuations which are independent of the Wess-Zumino term.

JHEP09(2009)032

characterizes a hypersurface of constant $r = r_\star$. At this point the Legendre transformed action vanishes on-shell. We will refer to it hereafter as the "singular shell". Calling r_h the radius of the horizon, one can easily see that $r_\star(E_p) \geq r_h$, and $r_\star(0) = r_h$. The Legendre transform of the DBI action is $\tilde{\mathcal{S}}_{\rm DBI} \sim -\int \mathrm{d}^{p+1}x\mathrm{d}r\tilde{\mathcal{L}}_{\rm DBI}$ with

$$\tilde{\mathcal{L}}_{\rm DBI} = -e^{-\phi}\sqrt{-(g_{00}g_{ii} + (2\pi\alpha')^2 E_p^2) g_{ii}^{p-1} g_{rr} g_{\Omega\Omega}^n}\sqrt{1 + \frac{(2\pi\alpha')^2(g_{00}n_q^2 + g_{ii}j_p^2)}{\mathcal{N}^2 e^{-2\phi} g_{00} g_{ii}^p g_{\Omega\Omega}^n}}\,. \tag{2.10}$$

Furthermore, as the quantity $g_{00}g_{ii} + {E_p}^2(2\pi\alpha')^2$ changes sign at $r = r_\star$, in order for (2.10) to remain real, we impose that the second square root in it also changes sign at $r_\star$. This leads to a relation[3] between j_p and E_p:

$$j_p = E_p\sqrt{\mathcal{N}^2 e^{-2\phi} {g_{ii}}^{p-2} g_{\Omega\Omega}^n + n_q^2(2\pi\alpha')^2 {g_{ii}}^{-2}}\Big|_{r_\star}\,, \tag{2.11}$$

and defining the conductivity as usual through Ohm's law, we get $\sigma = j_p/E_p$. This is the conductivity first found in [1] and the result is calculated purely in terms of background quantities. Although compact, the notation should not hide the important fact that σ is a non-linear function of E_p (see (3.5) below). This dependence arises from the evaluation of induced metric components at the singular shell $r_\star$. By studying linearized fluctuations on top of these background embeddings we will be able to extract information about properties of the gauge theory, and also calculate the conductivity using the Kubo formula. Agreement with the conductivity found in the macroscopic Ohm's law calculation (eq. 2.11) will be a good check of our methods (see section 4 for details).

3 Specializing to the $D3/D7$ system

In order to picture what is happening in the general Dp/Dq intersection we discuss here the possible embeddings in the case of the $D3/D7$ solution. In future sections we will discuss fluctuations about these solutions so we now introduce the coordinate system which will be made use of throughout. We find it convenient at this stage to use the radial variable, u, defined as $u = (r_h/r)^2$. The pullback metric of the $D7$-brane onto the $D3$-brane background will then be given by

$$\frac{ds^2}{R^2} = \frac{\pi^2 T^2}{u}\left((u^2-1)\mathrm{d}t^2 + \mathrm{d}\vec{x}_3^2\right) + \frac{(1-\psi^2+4u^2(1-u^2)\psi'^2)}{4u^2(1-u^2)(1-\psi^2)}\mathrm{d}u^2 + (1-\psi^2)\mathrm{d}\Omega_3^2\,, \tag{3.1}$$

where $u = u_b = 0$ corresponds to the UV of the gauge theory (the boundary of AdS) and $u = u_h = 1$ is the black hole horizon. The background field $\psi(u)$ corresponds to the classical

[3] it is interesting to note that in [23–25], a remarkably similar structure to the singular shell was observed in the trailing string solution, related to the local speed of light. Clearly the situations of a single moving quark and the quark current studied here are extremely similar. One can show that the infinite mass limit of the present current coincides with the current of a single quark moving through the plasma. We would like to thank C. Herzog and J. Casalderrey for pointing out this interesting observation.

JHEP09(2009)032

embedding of the $D7$-brane, and the gauge field, including transverse perturbations, is given by

$$A = A_0(u)\mathrm{d}t + (E_z\, t + A_z(u))\, \mathrm{d}z + \mathcal{A}_\perp(t, z, u)\mathrm{d}x_\perp\,, \tag{3.2}$$

with $x_\perp = \{x, y\}$. Here $A_0(u)$ corresponds to the non-zero baryon density, $A_z(u)$ to the non-zero current in the z-direction, and E_z is the finite electric field in the z direction. In this paper we will deal only with the transverse fluctuations, captured entirely in $\mathcal{A}_\perp(t, z, u)$ and defer the full investigation of the longitudinal and scalar modes for future study. The transverse sector decouples completely as we consider momentum in the direction parallel to the background electric field (see section 4 for further details). It is convenient to define the dimensionless electric field e as

$$e \equiv \frac{(2\pi\alpha')R^2}{(\pi T R^2)^2} E_z\,, \tag{3.3}$$

and constants of motion $\tilde{n}_q$ and $\tilde{\jmath}_z$, related to the charge density and current given in the previous section by

$$\begin{pmatrix} \tilde{n}_q \\ \tilde{\jmath}_z \end{pmatrix} \equiv \frac{4(2\pi\alpha')}{N_c N_f T^2\,(\pi T R^2)} \begin{pmatrix} n_q \\ j_z \end{pmatrix}\,. \tag{3.4}$$

However there is only one value of the current which renders a well defined action inside the singular shell. The position of the singular shell in this case is given by $u_\star = 1/\sqrt{1+e^2}$, and the current is found by demanding reality of the action across the singular shell, leading to

$$\tilde{\jmath}_z = e\sqrt{\sqrt{1+e^2}(1-\psi_\star^2)^3 + \frac{\tilde{n}_q^2}{1+e^2}}\,, \tag{3.5}$$

where $\psi_\star = \psi(u_\star)$. From this we can read off the electrical conductivity

$$\sigma = \frac{j_z}{E_z} = \frac{N_c N_f T}{4\pi}\frac{\tilde{\jmath}_z}{e} \equiv \frac{N_c N_f T}{4\pi}\tilde{\sigma}\,. \tag{3.6}$$

Using equation (3.5) we can express the background gauge fields $(A_0(u), A_z(u))$ entirely in terms of $\tilde{n}_q, e$ and the probe brane embedding profile $\psi(u)$

$$\begin{aligned} A_0'(u)^2 &= \frac{(\pi T R^2)^2 \tilde{n}_q^2 \left(1-u^2\left(1+e^2\right)\right)\left(1-\psi^2+4u^2\left(1-u^2\right)\psi'^2\right)}{4(2\pi\alpha')^2\,(1-\psi^2)\left((1-u^2)\,(1-\psi^2)^3 - u^3\left(\tilde{\jmath}_z^2 - \frac{2\tilde{n}_q^2}{1+e^2}\right) - u^5\tilde{n}_q^2\right)}\,, \\ A_z'(u)^2 &= \frac{\tilde{\jmath}_z^2}{\tilde{n}_q^2}\frac{A_0'^2}{(1-u^2)^2}\,. \end{aligned} \tag{3.7}$$

From here, $A_0(u)$ can be obtained by integrating from the horizon $u = 1$ with boundary condition $A_0(1) = 0$. The UV series solutions to these gauge fields are given by

$$A_0 = \mu - \frac{TR^2}{4\alpha'}\tilde{n}_q u + \dots\,, \tag{3.8a}$$

$$A_z = \frac{TR^2}{4\alpha'}\tilde{j}_z u + \dots\,, \tag{3.8b}$$

JHEP09(2009)032

μ being the chemical potential canonically conjugate to the baryon density.

The background field solution $\psi(u)$ corresponds to the classical embedding of the $D7$-brane. The range of this field is $0 \leq \psi(u) \leq 1$ and it is completely determined by its value either on the singular shell, or, for "Minkowski embeddings", the value of u for which this field goes to 1. The asymptotic behavior of the embedding near the UV gives the usual source (mass) and *vev* for the quark bilinear operator, leading to the relation that

$$\psi(u)_{u\to 0} \simeq \frac{m_q}{\sqrt{2}} u^{\frac{1}{2}} + \frac{c_q}{2\sqrt{2}} u^{\frac{3}{2}} . \tag{3.9}$$

The quark mass and condensate being given by

$$M_q = \frac{1}{2}\sqrt{g^2_{\rm YM} N_c} T m_q \,, \tag{3.10a}$$

$$\langle \bar{\Psi}\Psi \rangle = -\frac{1}{8}\sqrt{g^2_{\rm YM} N_c} N_f N_c T^3 c_q \,. \tag{3.10b}$$

Although this is really the source and *vev* of a supersymmetric operator [26], in the present case where supersymmetry is broken, both by the electric field and by the finite temperature, we will simply refer to the operator in question as the quark bilinear.

In what follows we shall plot the classical solutions to the embedding equation in a cartesian coordinate system in which it is more intuitive to picture the flows of the $D7$-brane. The change of variables between the original coordinates and those we will use to plot the solutions is

$$(\rho, L) = \left(\sqrt{1-\psi(u)^2}, \psi(u)\right) \frac{\sqrt{\sqrt{1-u^2}+1}}{\sqrt{u}},$$

Notice that $\psi = \cos\theta$ and the global factor defines an isotropic radial coordinate, $w(u) = \sqrt{\rho^2 + L^2}$, as used in many papers (see for example [22]).

For the $D7$ embedding in the finite temperature $D3$ geometry with finite electric field there are three families of solutions illustrated in figure 1. We discuss here the three types of behavior labelled "Minkowski solutions", "Black hole solutions" and "Conical solutions".

Minkowski solutions: these solutions do not intersect the singular shell and therefore do not meet the horizon. The current in this case is zero as there are no free charge carriers. For these solutions the energy supplied by the electric field is not sufficient to pair create quarks of such a high mass. They therefore only appear for sufficiently high values of m_q/T. Fundamental matter remains bound in long-lived mesons.

Minkowski solutions are labelled by the point of closest radial approach to the $D3$ branes, $u = u_{\rm max}$, at which they reach $\theta = 0$ or $\psi(u_{\rm max}) = 1$ with $u_h > u_\star \geq u_{\rm max}$. The second boundary condition needed to fix these solutions determines that there is no conical singularity at $u_{\rm max}$, corresponding to $\psi'(u_{\rm max}) = -\infty$.

Black hole solutions: these solutions pass smoothly through the singular shell and end on the black hole horizon without ever reaching $\psi(u) = 1$ for any value of u. The fact that the solutions pierce the singular shell indicates that there is a finite current. For these solutions, the quark mass is sufficiently small that the electric field can pair-create them.

JHEP09(2009)032

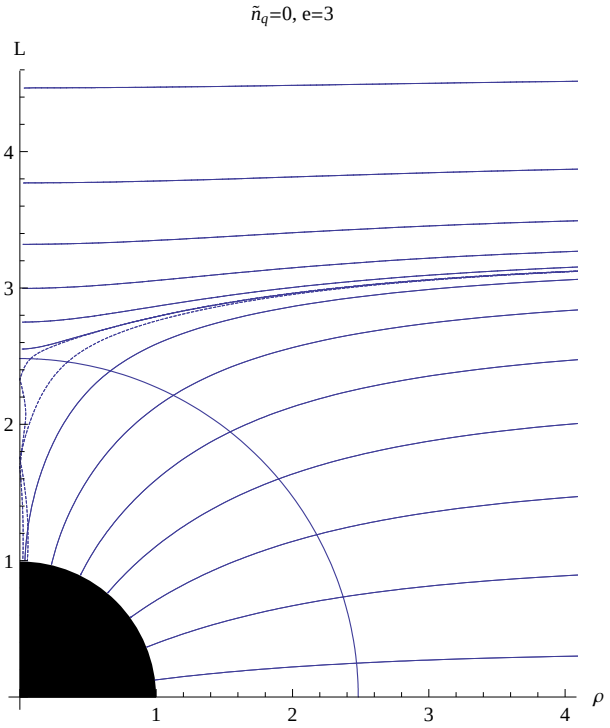

Figure 1. Embeddings at zero baryon density showing the Minkowski embeddings, which do not hit the singular shell (in this case at $\rho^2 + L^2 = 3 + \sqrt{10}$) conical embeddings given by short dashed lines which pass through the singular shell and hit the L-axis, and black hole solutions which pass smoothly from the singular shell to the horizon.

With these free charges a current can be set up. With an external electric field there is an unlimited supply of energy and one might have thought that the charge carriers would continue to accelerate. However, in the presence of the adjoint matter (with $N_f/N_c \to 0$) the energy of the fundamental matter is lost into this background and an equilibrium situation with a fixed, finite current is set up [1]. At finite baryon density all solutions have to end on the horizon (figure 2).

Conical solutions: these pass through the singular shell and appear to display a conical singularity at a radius, $u_{\rm cs} < u_h$, determined by $\psi(u_{\rm cs}) = 1$. We illustrate one of these solutions in figure 3 in the original u, ψ variables.

Solutions which pass through the singular shell are determined uniquely by specifying $\psi_\star = \psi(u_\star)$. All derivatives are fixed by this single boundary condition and the singular shell acts as an attractor for solutions[4]. This is reminiscent of the black hole horizon itself in the zero electric field situation, with which one can fix the behavior of a solution in the UV uniquely with a single boundary value.

[4]there are four solutions to the expansion about the singular shell, two of which are complex and one of which gives non-physical, oscillatory behavior.

JHEP09(2009)032

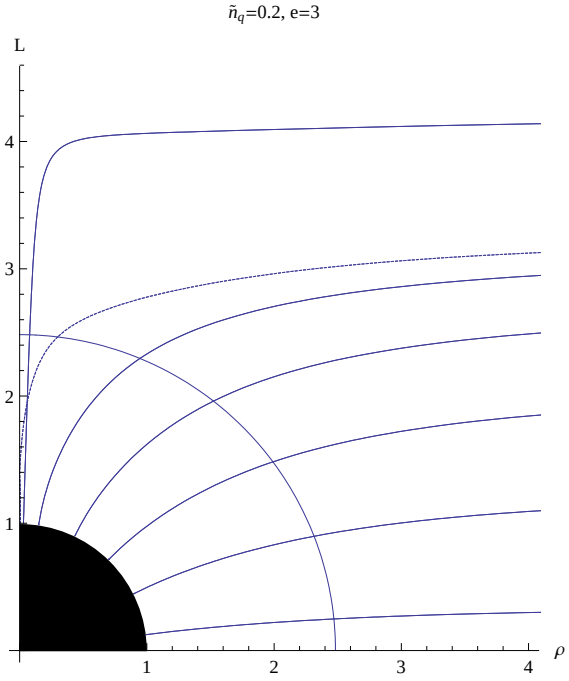

Figure 2. Embeddings at finite baryon density and the same electric field as in the previous figure illustrating the absence of Minkowski solutions. Note that there are still conical solutions in this case.

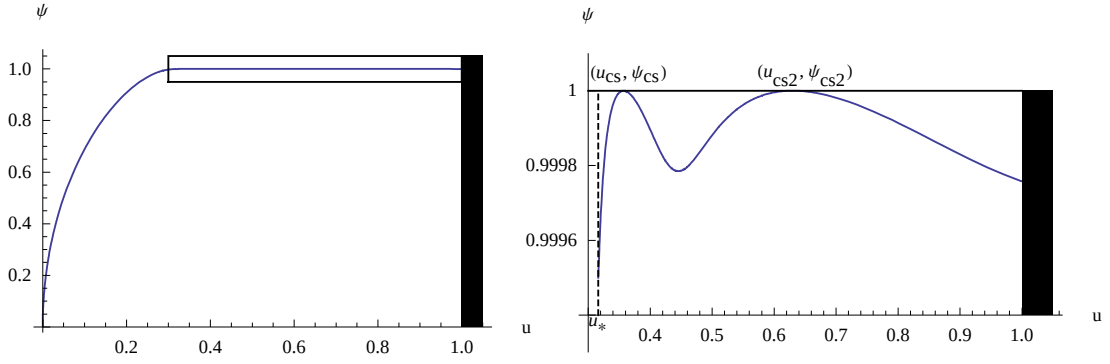

Figure 3. Example of a solution with two conical singularities. The left hand plot includes the whole range of the embedding from the UV ($u = 0$) to the horizon ($u = 1$). The second part focuses just on the region around the conical singularity, illustrated in the left hand plot by the boxed region. Here the first conical singularity is labeled as $(u_{\rm cs}, \psi_{\rm cs})$ while the second is labeled as (u_{cs2}, ψ_{cs2}). The L-axis is the line $\psi = 1$ while the horizon is marked as the black box. The singular shell is marked in the second plot as $u_\star$.

The electric field lines caused by the presence of free charges need to end somewhere and, hence, the brane must intersect the horizon. For the conical embeddings, the same

JHEP09(2009)032

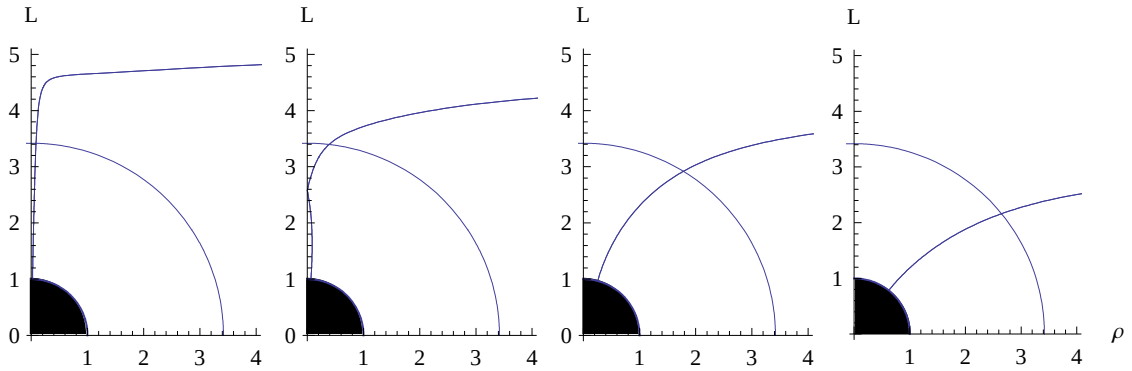

Figure 4. Evolution of the embedding profiles with decreasing values of the mass $m_q = 5$, 4.5, 4 and 3 at fixed values of $\tilde{n}_q = 0.05$ and electric field $e = 5.8$. After developing conical singularities the profile spreads suddenly for lower masses.

reasoning applies. Solving numerically we find that these solutions continue past the point of the conical singularity until they reach the horizon. Still, in (ρ, L) coordinates, at the points where they touch the L-axis one can observe that there is a jump in slope, hence the name conical singularity. After reaching this point, the value of ψ starts to decrease again, and the brane eventually hits the horizon (possible after encountering another conical singularity as illustrated in figure 3). By studying the tension of the $D7$-brane at the conical singularity we find that there is no other object which can be attached to the $D7$-brane matching it, meaning that the physical configuration is the one where the $D7$-branes continues through the conical singularity, eventually reaching the horizon.

3.1 Singular shell solutions

The solutions which pass through the singular shell exhibit subtle behavior which will influence much of the physics in what is to come. For this reason we will now discuss the details of the singular shell embeddings, parametrised by the three variables m_q, e and $\tilde{n}_q$.

Especially interesting is the behavior in the (m_q, e) plane. First we chose to fix the electric field and look at the solutions as a function of m_q.

In figure 4 we see the behavior for a range of masses. For the largest mass, $m_q = 5$, we see that there is a narrow throat, which leads from a relatively straight $D7$-embedding, sharply down into the singular shell and subsequently the horizon. As we decrease the mass to $m_q = 4.5$ we see that the behavior changes and we obtain a solution with a conical singularity. At this point the brane has a smoother profile and the sharp throat has disappeared. For still smaller masses than $m_q = 4$ we return to the pure black hole embedding and the conical singularity disappears. The profile is much smoother and there is a "wide throat" to the solution, rather than the previous sharp spike. Decreasing m_q still further widens this throat slowly and monotonically.

It should be noted that, with decreasing m_q, the conical solutions start with the conical singularity at the point where the black hole horizon meets the L-axis ($u = u_h$). The

JHEP09(2009)032

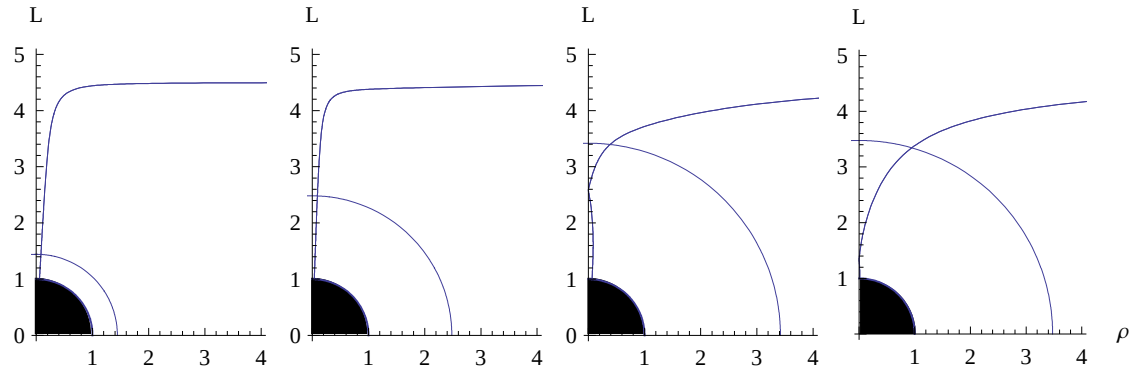

Figure 5. Evolution of the embedding profiles with the electric fields $e = 0.8, 3, 5.8$ and 6 at fixed values of $\tilde{n}_q = 0.05$ and quark mass $m_q = 4.5$. We observe the developement of conical embeddings in the range $e \in (5.7, 6)$. Increasing the value of e there is a sudden change in form, and the profiles spread significantly.

position $u_{\rm cs}$ of the first conical singularity (for there may be multiple) moves away from the horizon and then returns to it as the quark mass is decreased further.

We see from this example that over a small range of masses there is a very fast change in behavior, from a sharp spike solution, through a conical solution, to a smooth, wide throat solution. This behavior is generic, though the region over which this fast transition occurs is dependent on both m_q and e. Indeed not all values of $\tilde{n}_q$ and e will exhibit conical solutions.

Keeping m_q fixed and varying e gives a similar behavior, exhibited in figure 5. We label the region where the behavior changes quickly as a function of m_q or e the "crossover region" (which may be a genuine crossover or a true phase transition). As stated above, this region may or may not contain a subregion of conical singular solutions, depending on the value of $\tilde{n}_q$.

As a physical motivation for such a fast change in behaviour it seems that there are two competing mechanisms forcing the brane embedding to go in two different directions. The crossover region is defined as the region where one of of these effects becomes dominant over the other and there is a sudden change in the behavior. This is rather reminiscent of the two effects seen in the expression for the conductivity, one of which becomes more important as e increases and one of which becomes more important as it decreases. These two terms are related to the the pair-creation and presence of free charges respectively.

We can plot the crossover region in the (m_q, e) plane in which conical solutions are present. This wedge is shown in figure 6 for varying values of $\tilde{n}_q$ corresponding to the increasingly dark colors. It is rather peculiar that the only effect of the baryon density is to shift the starting point within the same region and not to displace the region at all in some direction.

JHEP09(2009)032

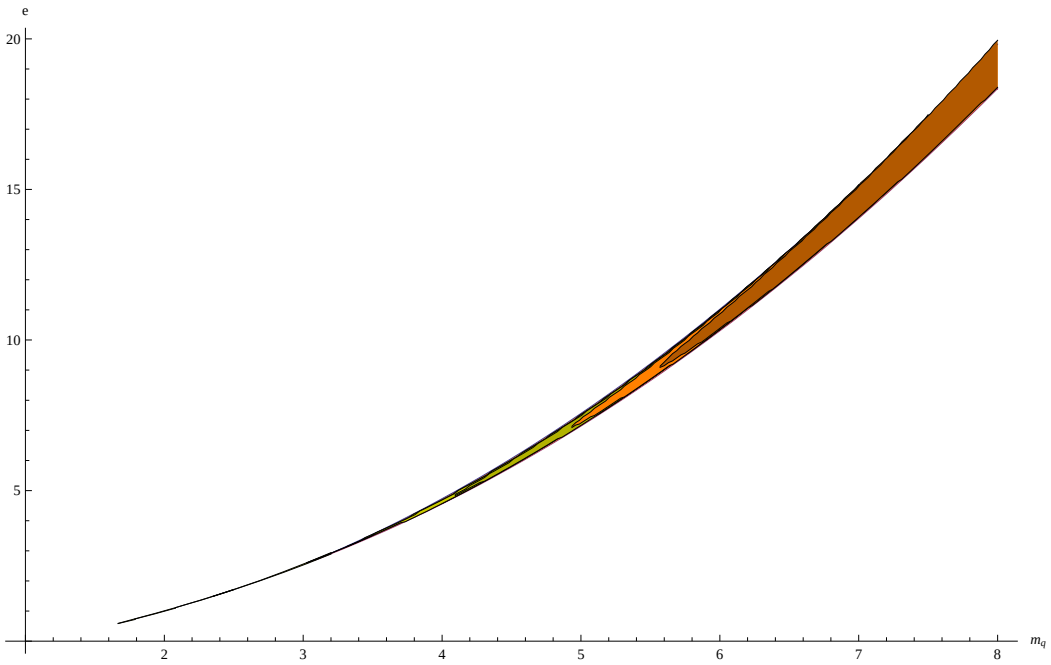

Figure 6. The shaded region is where conical embeddings are found in the plane (m_q, e). The regions for different $\tilde{n}_q$ are superimposed, beginning at larger m_q the larger $\tilde{n}_q$ is. The lowest region is for $\tilde{n}_q = 2 \cdot 10^{-5}$ and this contains all other regions for larger values of n_q. The orange region is for $\tilde{n}_q = 0.6$ and the brown one corresponds to $\tilde{n}_q = 1.2$.

3.2 Multivalued embeddings and phase transitions

For nonvanishing baryon number all solutions are of the "singular shell" type, either black hole or conical. Therefore, they all pierce the singular shell at a specific value of $\psi_\star = \psi(r_\star)$. In fact, from the numerical point of view, the specification of $\psi_\star$ is all that is needed in order to integrate numerically outwards from $r = r_\star$ to $r = \infty$. In other words, embeddings are single valued functions of $\psi_\star$. This is to be contrasted with the dependence with the mass m_q. For specific values of the baryon number $\tilde{n}_q$ and the electric field e, there will be more (typically three) embeddings that share the same value of the asymptotic mass m_q. The easiest way to see this is to plot m_q as a function of the parameter $\psi_\star$. This can be seen in figure 7. For a large enough value of $\tilde{n}_q$ at a given electric field we find the left-most graph. Here we see that there is no multivaluedness in the quark mass. The middle graph marks the critical value of $\tilde{n}_q$ where multivaluedness begins. This value marks the point of a second order phase transition. For a low enough value of the baryon density, $\tilde{n}_q$, at a given electric field, e, we find the right-most curve. Here we see a range of values of m_q for which three different embeddings (i.e. values of $\psi_\star$) are possible. On general grounds, we also expect that all the observables will inherit this multivaluedness. In particular the condensate $c_q(m_q)$ will also be multivalued simply because each one of the three profiles that share the common value of m_q have different subleading asymptotics. Physically, only one of the three embeddings can be the true vacuum of the theory, and a transition will

JHEP09(2009)032

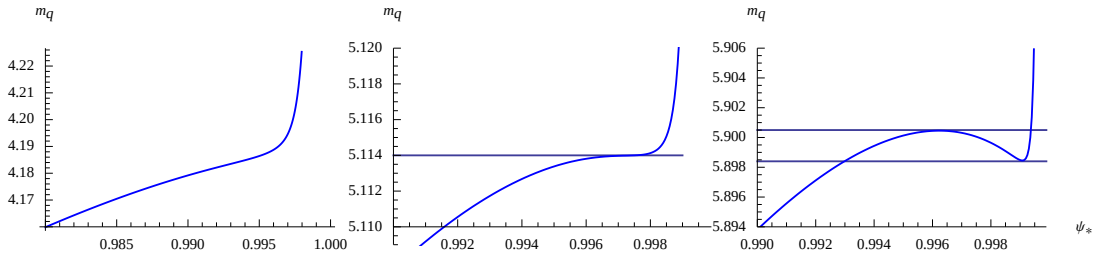

Figure 7. Three curves $m_q(\psi_*)$ at values of $\tilde{n}_q = 0.1$ and electric fields $e = 5, 7.5$ and 10 respectively. At $e = 5$, the left-most graph shows no phase transition. At $e = 7.5$ a second order phase transition occurs at $m_{q,tr} = 5.114$ as seen in the middle graph. At $e = 10$ we see the first order phase transition for a value $m_{q,tr} \in (5.898, 5.900)$ in the right-most graph. In all of these we zoom in on the region of interest.

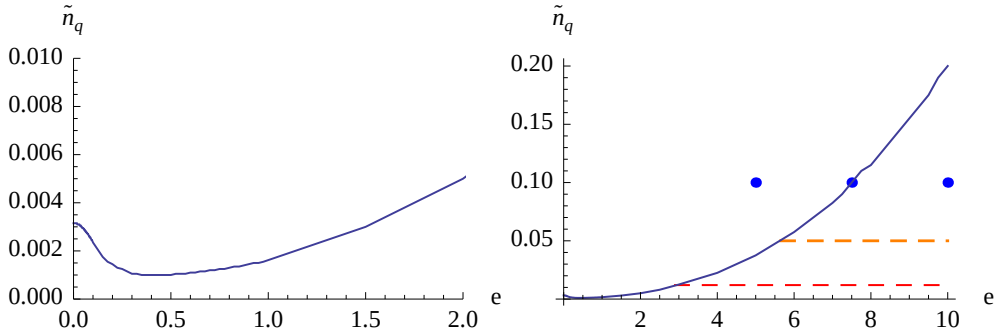

Figure 8. The line of second order phase transitions in the $(e, \tilde{n}_q)$ plane. Below this line there exist first order phase transitions at a particular value of the quark mass. The three blue dots correspond to the three plots in figure 7 while the red and orange dashed lines correspond to the equivalent lines in figure 9.

take place for a critical value $m_{q,tr}$.[5] The transition value $m_{q,tr}$ can be obtained either by minimizing the free energy, or by means of the "equal area law" applied to, say, the $c_q(m_q)$ curve. First order phase transitions occur only for a given region in the $(\tilde{n}_q, e)$ plane. For example, at zero electric field the first order phase transition only exists for $\tilde{n}_q < 0.00315$ [17]. This value marks the critical point and thus a second order phase transition. As a function of the electric field strength this critical point defines a line in the $(\tilde{n}_q, e)$ plane and this critical line is plotted in figure 8. Below this curve there are multivalued functions $m_q(\psi_\star)$ and correspondingly a first order phase transition at a given value of the mass $m_{q,tr}$. The three curves shown in figure 7 are in one to one correspondence with the three blue dots in figure 8, one above the critical line, with no phase transition, one on the critical line with a second order phase transition, and one below the critical line with a first order phase transition. We observe that the effect of the electric field (above $e \sim 0.5$) is to enhance significantly the area of first order phase transitions.

[5] This can be thought as a transition as a function of temperature, as $m_q = \bar{M}/T$

JHEP09(2009)032

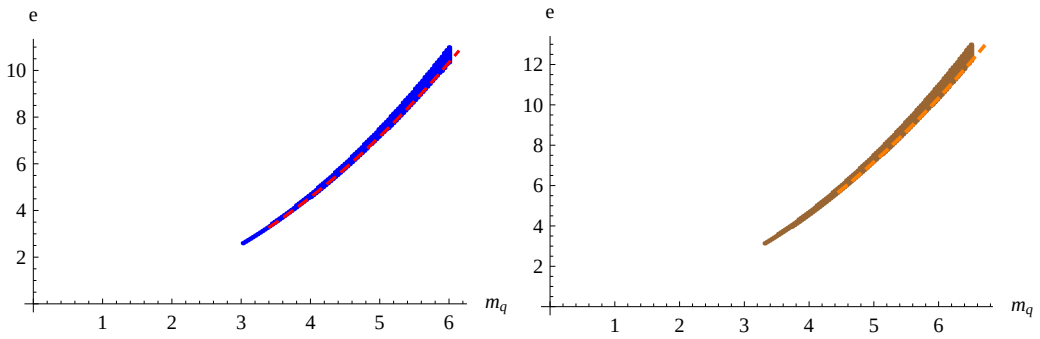

Figure 9. The blue (brown) regions are values for which conical embeddings are found at fixed values of $\tilde{n}_q = 0.012$ (0.05). The red (orange) lines are also very thin wedges where the three embeddings are possible, hence where $m_q(\psi_\star)$ is a multivalued function. On this scale these regions of possible instability are indistinguishable from one dimensional lines. This can be seen by looking at the right most plot in figure 7 where the width of the region of multivaluedness in m_q is of the order 0.002.

We know that in the region of multivaluedness (e.g. the ones with m_q between the two straight lines in the right-most graph in figure 7) there are potentially unstable embeddings. We would like to compare the region in the (m_q, e) plane where the multivaluedness of $m_q(\psi_\star)$ occurs with that of conical embeddings. This region of multivaluedness appears as a very thin wedge in the (m_q, e) plane. This wedge coincides with the lower edge of the region of conical embeddings shown in figure 6. In figure 9 we exhibit the regions of conical embeddings and multivaluedness for $\tilde{n}_q = 0.012$ and 0.05 respectively. One observes that for large enough electric field they are contained within the region of conical embeddings. At zero electric field we know that this can not be so as there are no conical embeddings. We find that for $e \lesssim 1.1$ the multivalued solutions do not lie within the region of conical embeddings. On the other hand, there exist conical embeddings which are specified by a unique value of m_q. In order to study the stability of these embeddings, a full thermodynamic analysis of this system is needed. We postpone this discussion for a future paper. It is tempting to conjecture a relation between the shaded areas in 9 and the one in figure 2 of [17]. Following this conjecture we assume that the region of conical embeddings and nearby in the parameter space may be unstable and this should be accounted for in the following sections. In the subsequent analysis, we mark this region of possible instabilities with dashed lines corresponding to the line of conical embeddings. Such a stability analysis will involve the study of tachyonic quasinormal modes on top of the classical embedding solutions.

3.3 Chiral condensate

Having detected a crossover region (again, which may include both crossovers and phase transitions), given by a sudden change in the behavior of probe embeddings, it is natural to expect that other physical quantities will be affected. In the present section we will examine the chiral condensate.

JHEP09(2009)032

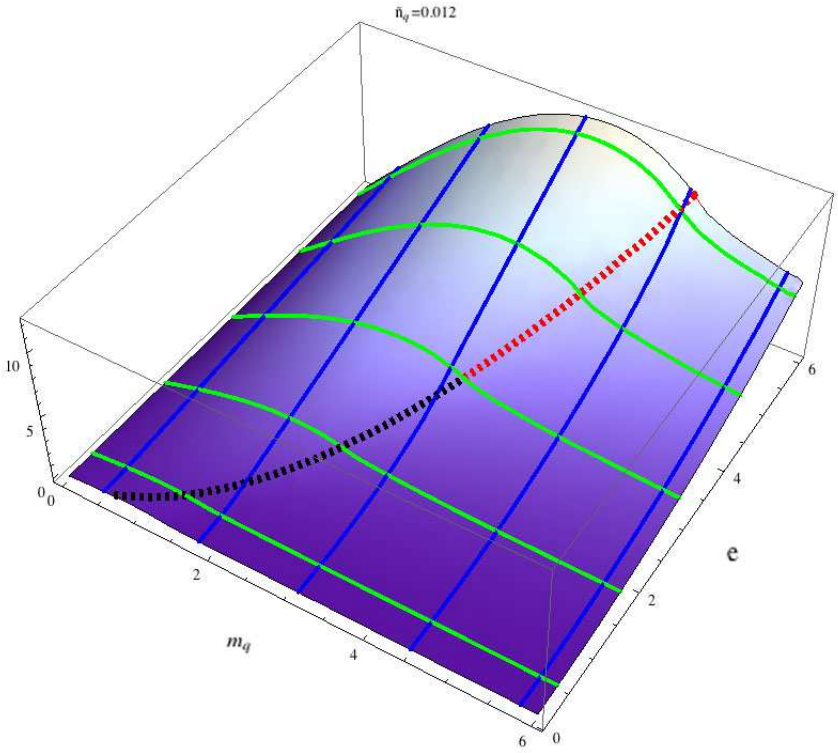

Figure 10. Condensate c_q as a function of electric field and mass for $\tilde{n}_q = 0.012$. Curves of constant m_q are plotted in blue, and those of constant e in green. We superimpose a dashed curve where a transition and a change in behaviour is observed. Across the black segment the transition is a crossover that occurs through conical embeddings. For higher e, upon crossing the red segment the transition is of first order and the same multivaluedness of c_q as a function of m_q is observed. Actually the red segment is the same as the one that can be seen in figures 8 and 9.

We plot $-c \sim \langle\bar{\Psi}\Psi\rangle$ given by equation (3.10) as a function of m_q and e for $\tilde{n}_q = 0.012$ in figure 10. We see that in the region where the crossover in behavior occurs at the singular shell the condensate also undergoes a faster change in behavior, as compared with other regions in the (m_q, e) plane. We have superimposed on the graph the curve $e = 0.29\, m_q^2$ which runs through the middle of the orange region in figure 6. We see that this curve coincides roughly, as expected, with the region where the level curves change from concave to convex. We should note however that the change in behavior of the chiral condensate over the crossover region is much less pronounced than that of many other quantities as we will show.

3.4 Charge susceptibility

Another physically relevant quantity showing a fast change in behavior across the crossover region described in the previous sections is the charge susceptibility, thermodynamically

JHEP09(2009)032

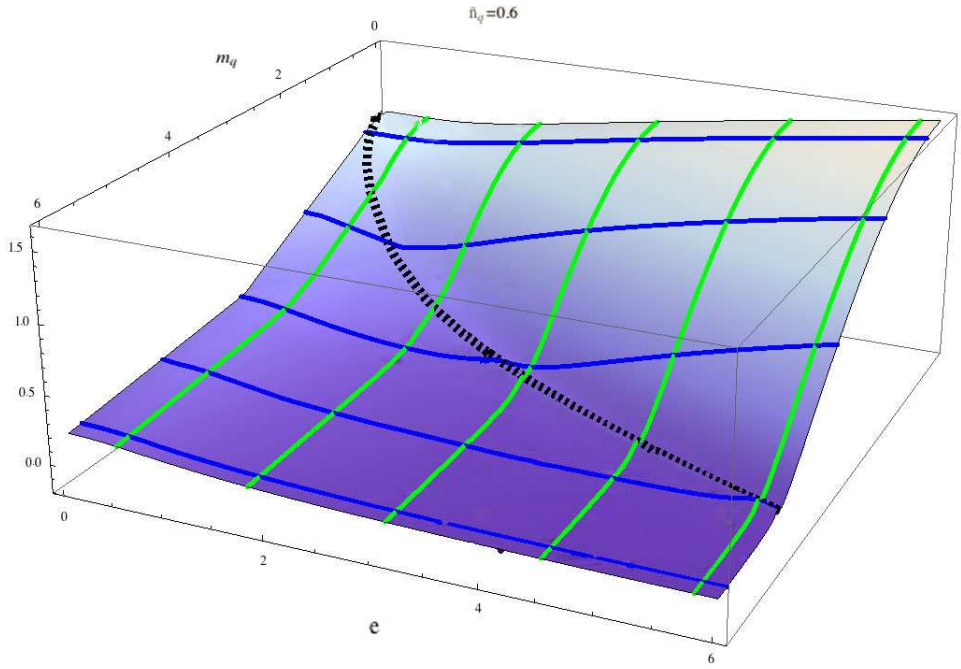

Figure 11. Dimensionles charge susceptibility $\tilde{\Xi}$ as a function of the quark mass and electric field for $\tilde{n}_q = 0.6$. Green, blue and black lines have the same meaning as in the figure for the chiral condensate.

defined as

$$\Xi = \left.\frac{\partial n_q}{\partial \mu}\right|_T = \frac{N_c N_f T^2}{2} \left.\frac{\partial \tilde{n}_q}{\partial \tilde{\mu}}\right|_T \equiv \frac{N_c N_f T^2}{2} \tilde{\Xi}, \tag{3.11}$$

where μ is defined[6] in equation (3.8a). From eq. (2.9a) we can read the dependence of μ on the charge density at fixed temperature and extract the value of the susceptibility. In figure 11 we plot this quantity as a function of the quark mass and the electric field for $\tilde{n}_q = 0.6$. There we can see that in the region where we have narrow throats in the embedding profiles the susceptibility varies very slowly. On the other hand, in the region with wide-throat profiles we have a more pronounced slope. These two regions are separated by the line where conical embeddings may occur. We will find this behavior again, when considering the conductivity and the photoproduction.

3.5 Conductivity

In [1], by analyzing eq. (3.6) it was conjectured that the two terms present under the square root have physically clear and distinct origins. The second one is the clearest, as it is directly related to the presence of charge carriers proportional to the net baryon charge $\tilde{n}_q$. Notice the presence of the electric field in the denominator, which suppresses this contribution for larger values of e. The first one should correspond to the presence

[6] where we have defined $A_0 = \frac{TR^2}{4\alpha'}(\tilde{\mu} - \tilde{n}_q u + \cdots)$ from equation (3.8a).

JHEP09(2009)032

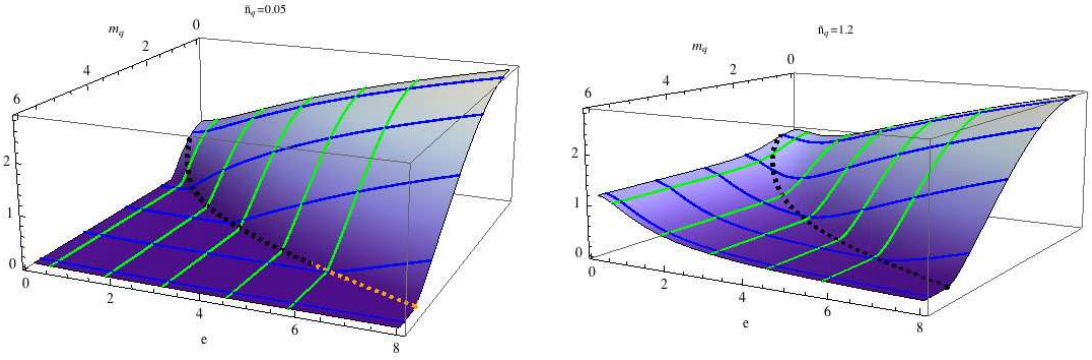

Figure 12. Dimensionless conductivity, $\tilde{\sigma}$, as a function of e and m_q for two different values of $\tilde{n}_q = 0.05$ and 1.2. Varying m_q at constant e shows a stronger change in slope upon crossing the black line than varying e. Similarly to figure 10, we have superimposed the black dashed curve of conical embeddings, and for high enough e, in orange, the segment of first order phase transitions. This segment is in correspondence with the similar one in figures 8 and 9.

of charge carriers that come from pair production from the vacuum. It is enhanced by a stronger electric field, and, assuming a direct relation between ψ_* and the mass, this term should vanish for high enough masses. Roughly speaking, this behavior is seen in the set of graphs shown in figure 12.

What is less obvious is the sharpness of the transition to the region of high conductivity dominated by the first term in (5.5). This is the slope which is visible for high values of e and low values of m_q. Clearly the abruptness in this transition comes from the hidden dependence of $\psi_\star$ on e and m_q, and the sudden change in profiles that was investigated in the previous section is clearly behind this strong sensitivity.

3.6 Charge diffusion

A formal study of the charge diffusion for this system would involve solving for the longitudinal vector channel, that presents a pole in its correlator which, in the hydrodynamic limit, gives information about this transport coefficient. In this paper we do not follow this procedure but exploit the Einstein relation, which expresses the diffusion as the quotient of the conductivity by the susceptibility

$$D = \frac{\sigma}{\Xi} = \frac{1}{2\pi T}\frac{\tilde{\sigma}}{\tilde{\Xi}} \equiv \frac{\tilde{D}}{2\pi T}\,. \tag{3.12}$$

With our numerical methods we are able to recover the vanishing electric field results of [27], and in figure 13 we show how these get modified in the presence of a finite electric field for $\tilde{n}_q = 0.6$.

In this figure we can see an interesting behavior. Keeping the electric field fixed and studying the diffusion constant when the quark mass increases we first see that it decreases very slowly until one reaches the crossover region. Once this happens there is first a rapid decrease and, once we pass this region and enter the parameter space where we have

JHEP09(2009)032

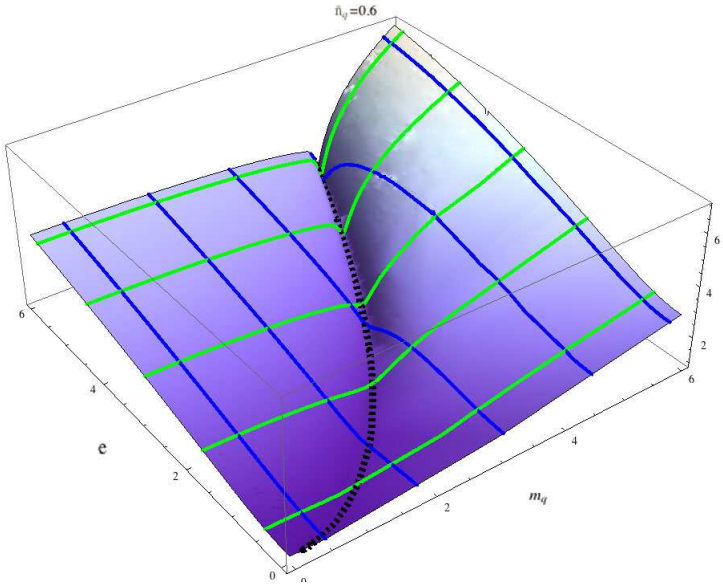

Figure 13. Dimensionless charge diffusion $\tilde{D}$ as a function of the quark mass and electric field for $\tilde{n}_q = 0.6$.

narrow-throat embedding profiles, we find that the diffusion constant increases with the quark mass very fast. This rapidly changing behavior with the mass is correlated with the vanishing of the susceptilibity in the same limit.

4 Fluctuations

In order to compute current-current correlators we must consider perturbations of the gauge field $\mathcal{A}_\mu$. The components $\mathcal{A}_0$ and $\mathcal{A}_p$ are scalars under the little group $O(p-1)$, and will mix with any other scalar modes present in the system, for example the profile fluctuation $\delta\psi$ or fluctuations of the dilaton $\delta\phi$. This channel is fairly complicated to analyse and for the D3/D7 case it has been studied in the absence of electric field in [19]. On the other hand transverse fluctuations $\mathcal{A}_\perp = \mathcal{A}_i$ with $i = 1, \ldots, p-1$ will transform as vectors, and hence decouple completely from all other excitation modes and have been studied, again in the absence of an electric field, in [28]. In this paper we will be concerned exclusively with these transverse fluctuations, leaving the coupled sector for future study.

In a rotationally invariant theory, the retarded Green's function $G^R_{\mu\nu}$ involving perturbations of the form $\exp(-ik_\mu x^\mu)$ is generically split into two different polarization tensors [29]

$$G^R_{\mu\nu}(k) = P^\perp_{\mu\nu}(k)\Pi^\perp(k) + P^{||}_{\mu\nu}(k)\Pi^{||}(k)\,, \tag{4.1}$$

where the projectors are defined as $P^\perp_{00} = P^\perp_{0m} = 0$, $P^\perp_{mn} = \delta_{mn} - k_m k_n/\vec{k}^2$, $P^{||}_{\mu\nu} = \eta_{\mu\nu} - k_\mu k_\nu/k^2$. In the present setup we expect this structure to remain unaltered as long as the background electric field, E_p, points in the same direction, x^p, as the propagation of the perturbation and, hence leaves the $O(p-1)$ invariance untouched. For the transverse

JHEP09(2009)032

fluctuations, the components of G^R_{rs} for $r,s = \{1,\ldots,p-1\}$ are related directly to $\Pi^\perp$ by

$$G^R_{rs}(k) = \delta_{rs}\Pi^\perp(k)\,. \tag{4.2}$$

The prescription for the Lorentzian correlator relates the polarization function $\Pi^\perp(k)$ to the boundary action for the transverse fluctuations

$$S_{\rm bou} = -\frac{\mathcal{N}}{2}\int_{r\to r_b} \mathrm{d}^{p+1}x\, e^{-\phi}\sqrt{-\gamma}\gamma^{\perp\perp}\gamma^{rr}\mathcal{A}'_\perp\mathcal{A}_\perp\,, \tag{4.3}$$

with $\mathcal{N}$ defined as in equation (2.9). This prescription gives [30]

$$\Pi^\perp = \mathcal{N}e^{-\phi}\sqrt{-\gamma}\gamma^{\perp\perp}\gamma^{rr}\frac{\mathcal{A}'_\perp\mathcal{A}^*_\perp}{|\mathcal{A}|^2}\bigg|_{r\to r_b}\,. \tag{4.4}$$

In section 5 we discuss further how to calculate this quantity for the specific case of the $D3/D7$ system.

4.1 Transport phenomena

The conductivity is defined macroscopically via Ohm's law as the ratio between the current density and the field that creates that flow of current. The calculation of the conductivity for a Dp/Dq intersection has been done following this definition in [1]. Here we are interested in a microscopic derivation using the Kubo relation:

$$D\Xi = -\lim_{\omega\to 0}\frac{\mathrm{Im}\Pi^\perp(\omega=q)}{\omega}\,, \tag{4.5}$$

where D is the diffusion constant and Ξ the susceptibility of the medium. In the next section we will show that this prescription leads to the same analytical expression obtained in [1], thereby proving the validity of the Einstein's relation $\sigma = D\Xi$. An independent check of this relation amounts to calculating the susceptibility Ξ and the diffusion constant D separately.

The susceptibility is an equilibrium quantity given by a thermodynamic definition $\Xi = \partial n_q/\partial\mu\big|_T$, where μ is the chemical potential and n_q the charge density, as has been discussed in section 3.4. On the other hand, the diffusion constant, D, can be obtained from a hydrodynamic pole in the correlator for the longitudinal channel of vector fluctuations, relating the frequency and the momentum as dictated by Fick's law: $\omega = -iDq^2 + \mathcal{O}(q^3)$, although we leave this calculation for the future. Numerically one can see that in the case of vanishing electric field the product $D\Xi$ obtained in this way agrees with σ, as explicitely shown in [27].

4.2 Gauge field fluctuations

At this point we must study what boundary conditions we need to impose on the transverse fluctuations at any singular points in their equations of motion. The equation of

motion for the transverse fluctuations after inserting the plane wave ansatz $\mathcal{A}_\perp(t,\vec{x},r) \to e^{-i(\omega x^0 - q x^p)}\mathcal{A}_\perp(r)$ reads

$$\begin{aligned}
&\partial_r\left[e^{-\phi}\sqrt{-\gamma}\gamma^{\perp\perp}\left(\gamma^{rr}\mathcal{A}'_\perp - i\left(\omega\gamma^{(0r)} - q\gamma^{(pr)}\right)\mathcal{A}_\perp\right)\right] \\
&\quad -ie^{-\phi}\sqrt{-\gamma}\gamma^{\perp\perp}\left(\omega\gamma^{(0r)} - q\gamma^{(pr)}\right)\mathcal{A}'_\perp \\
&\qquad -e^{-\phi}\sqrt{-\gamma}\gamma^{\perp\perp}\left(\omega^2\gamma^{00} + q^2\gamma^{pp}\right)\mathcal{A}_\perp + 2\,\omega\,q\,e^{-\phi}\sqrt{-\gamma}\gamma^{\perp\perp}\gamma^{(0p)}\mathcal{A}_\perp = 0\,. \qquad (4.6)
\end{aligned}$$

At finite temperature we need to make sure that the solution is regular at the horizon[7]. This can be achieved by performing a Frobenius expansion. The solution is regularised as $\mathcal{A}_\perp(r) = (r-r_h)^{\eta^{(h)}}\mathcal{A}_{\perp,reg}$ where the indices are found to be

$$\eta^{(h)}_\pm = \frac{1\pm 1}{2} - i\,\frac{\omega}{4\pi T}\,, \qquad (4.7)$$

the (h) indicating that this is an index at the horizon. Note that this is markedly different from the case of zero electric field where the only possibilities were outgoing or incoming boundary conditions. Now there is the possibility of an additional damping factor at the horizon. In this case the choice of outgoing or incoming boundary conditions is dependent on the relative sign between A'_0 and A'_p. In our choice of the background gauge fields (equation (2.9)) we have chosen the relative sign of these to give the appropriate incoming wave condition.

In addition to the singular behavior at the horizon, there is also a singularity in the equations of motion for the fluctuations at the singular shell, $r_\star$. We can perform a similar Frobenius study in this region. In this case we find one trivial index, $\eta^{(\star)}_0 = 0$, while the other, $\eta^{(\star)}_r$, is a very complicated function of E_p, ω, n_q and $\psi_\star$ which, in the limit of vanishing electric field, is given by $\eta^{(\star)}_r(E_p\to 0) = i\frac{\omega}{2\pi T}$.

Finally, in order to choose our boundary conditions we want to recover the usual expression for the indices at the horizon in the limit of $E_p \to 0$. Notice that in this limit, as we have already seen, $r_\star \to r_h$, so

$$(r-r_h)^{\eta^{(\lim)}} \equiv \lim_{E_p\to 0}(r-r_h)^{\eta^{(h)}}(r-r_\star)^{\eta^{(\star)}} = \lim_{E_p\to 0}(r-r_h)^{\eta^{(h)}+\eta^{(\star)}} \stackrel{?}{=} (r-r_h)^{\pm i\frac{\omega}{4\pi T}}\,. \qquad (4.8)$$

We have four possible combinations of the two values at the horizon and at the singular shell, combining to give the following values for $\eta^{(\lim)}$. From table 1 we can see that to perform our study with a consistent $E_p \to 0$ limit we have to take the horizon index $\eta^{(h)}_-$ and at the singular shell $\eta^{(\star)}_0$.

As a further check that we chose the correct index at the singular shell we will show that our choice is the unique one that recovers the conductivity (2.11) via the Kubo formula (4.5).

[7] provided a non vanishing n_q the branes can be black hole-type or conical-type. They touch the black hole horizon at some point, and the formula obtained will be shown to coincide with numerics also for conical-type embeddings.

JHEP09(2009)032

$\eta^{(lim)}$	$\eta_+^{(h)}$	$\eta_-^{(h)}$
$\eta_0^{(\star)}$	$1 - i\,\frac{\omega}{4\pi T}$	$-i\,\frac{\omega}{4\pi T}$
$\eta_r^{(\star)}$	$1 + i\,\frac{\omega}{4\pi T}$	$i\,\frac{\omega}{4\pi T}$

Table 1. The four possibilities for the index on the horizon, $\eta^{(lim)}$, in the limit of vanishing electric field.

4.2.1 Fluctuations in the hydrodynamic approximation

Here we are interested in solving equation (4.6) in the limit of vanishing momentum. It is a consistency check that the solutions are regular both at the horizon and at the singular shell.

In the hydrodynamic limit we can expand the transverse fluctuation in a series in small ω and q. In order to perform this expansion we set $(\omega, q) \to \lambda_{\rm hyd}(\omega, q)$ and perform the expansion for small $\lambda_{\rm hyd}$. The series for the fluctuation then reads

$$\mathcal{A}_\perp = \mathcal{A}_\perp^{(0)} + \lambda_{\rm hyd}\,\mathcal{A}_\perp^{(1)} + \mathcal{O}(\lambda_{\rm hyd}^2)\,. \tag{4.9}$$

With the indices chosen in the last section we can write down the regular functions in the bulk order by order. At leading order in the hydrodynamic limit we calculate the equation of motion for the transverse gauge field fluctuation (4.6) and find

$$\left(e^{-\phi}\sqrt{-\gamma}\gamma^{\perp\perp}\gamma^{rr}\mathcal{A}_\perp^{(0)\prime}\right)' = 0\,. \tag{4.10}$$

This has a closed solution given by

$$\mathcal{A}_\perp^{(0)}(r) = C_0 + C_1\int_{r_h}^{r}\frac{\mathrm{d}\tilde{r}}{e^{-\phi}\sqrt{-\gamma}\gamma^{\perp\perp}\gamma^{rr}}\,. \tag{4.11}$$

where the integral is taken from the horizon out to a radius r. This integral is divergent at the singular shell and so the only regular solution is the the constant one $\mathcal{A}_\perp^{(0)}(r) = C_0$.

Calculating the equation for the fluctuation at next to leading order we obtain the following equation

$$\left(e^{-\phi}\sqrt{-\gamma}\gamma^{\perp\perp}\gamma^{rr}\mathcal{A}_\perp^{(1)\prime}\right)' - i\omega\left(e^{-\phi}\sqrt{-\gamma}\gamma^{\perp\perp}\gamma^{(0r)}C_0\right)' = 0\,, \tag{4.12}$$

which can be integrated twice to give

$$\mathcal{A}_\perp^{(1)}(r) = \int_{r_h}^{r}\frac{C_1 + i\omega e^{-\phi}\sqrt{-\gamma}\gamma^{\perp\perp}\gamma^{(0r)}C_0}{e^{-\phi}\sqrt{-\gamma}\gamma^{\perp\perp}\gamma^{rr}}\mathrm{d}\tilde{r} + C_2\,. \tag{4.13}$$

This expression is completely regular at the horizon but needs to be regularized at the singular shell. With this regularity condition we obtain

$$C_1 = -i\omega\frac{j_p C_0}{\mathcal{N}E_p}\,. \tag{4.14}$$

JHEP09(2009)032

We now calculate the conductivity from the Kubo relation (4.5), which relates the transport coefficient to the transverse correlation function. Using this prescription we obtain:

$$\sigma = -\mathcal{N} \lim_{\omega\to 0} \mathrm{Im}\, \frac{C_1 + i\omega e^{-\phi}\sqrt{-\gamma}\gamma^{\perp\perp}\gamma^{(0r)}C_0}{\omega C_0}\bigg|_{r_{\rm bou}} = \frac{j_p}{E_p}\left(1 + \frac{(2\pi\alpha')^2 {E_p}^2}{g_{00}g_{ii}}\right)\bigg|_{r_{\rm bou}}, \tag{4.15}$$

The second term vanishes when evaluated at the boundary and we recover the result of [1]. This is a good clue that we have chosen the correct index at the singular shell. Had we chosen the index $\eta_r^{(\star)}$ we would have found a different answer (incompatible with the result of the macroscopic conductivity calculation), which in the limit of vanishing electric field reads $\sigma_{E_p=0} = -\lim_{E_p\to 0} j_p/E_p$, exhibiting a change of sign that can be traced back to the time reversal that also appears in table 1. With this positive result in hand we can now go on to calculate the spectral function away from the hydrodynamic limit which will ultimately give us the photoproduction of the strongly coupled plasma in the presence of an external electric field.

5 Fluctuations in the $D3/D7$ system

Here we specialise once again to the $D3/D7$ system and turn to numerical calculations of physically relevant quantities. Having shown that our choice of indices is the unique one to recover the conductivity while also recovering the correct $E_p \to 0$ limit (the usual incoming wave boundary conditions) we are now able to study the spectral function for mesons dissociated both by the electric field and by finite temperature effects.

Using the radial coordinate introduced in section 3, the gauge field can be expanded in the UV (small u region) in terms of the two independent solutions

$$\mathcal{A}_\perp = \mathcal{B}_1\mathcal{A}^{(1)}(u) + \mathcal{B}_2\mathcal{A}^{(2)}(u)\,, \tag{5.1}$$

where

$$\mathcal{A}^{(1)}(u) = 1 + \sum_{i=2}^{\infty} a_i^{(1)} u^i + h\,\mathcal{A}^{(2)}\log u\,, \tag{5.2a}$$

$$\mathcal{A}^{(2)}(u) = u + \sum_{i=2}^{\infty} a_i^{(2)} u^i\,. \tag{5.2b}$$

All the coefficients $a_i^{(n)}$ and h are determined by recursion relations[8], where $\mathcal{B}_m$ are the two connection coefficients. Applying the lorentzian AdS/CFT prescription (eq. (4.4)) we find for the two-point function

$$\Pi^\perp = \frac{N_c N_f T^2}{2}\lim_{u\to 0}\frac{\mathcal{A}_\perp{}'(u)}{\mathcal{A}_\perp(u)} = \frac{N_c N_f T^2}{2}\left(\frac{\mathcal{B}_2}{\mathcal{B}_1} + h\,(1 + \log(u\to 0))\right), \tag{5.3}$$

[8] for example $h = \mathfrak{q}^2 - \mathfrak{w}^2$ with $\mathfrak{w} \equiv \omega/(2\pi T)$ and $\mathfrak{q} \equiv q/(2\pi T)$.

leading to an expression for the transverse part of the spectral function

$$\chi^{\perp} = -2\,\mathrm{Im}\,\Pi^{\perp} = -N_c N_f T^2\,\mathrm{Im}\,\frac{\mathcal{B}_2}{\mathcal{B}_1} \equiv N_c N_f T^2 \tilde{\chi}^{\perp}\,. \tag{5.4}$$

This of course will be a function of $e, \tilde{n}_q$ and m_q leading to a large parameter space. We split this analysis into two separate areas: The first is confined to solutions with zero spatial momentum which will allow us to see the appearance of quasiparticle like peaks in certain limits of the parameter space, and also to compute the conductivity numerically as the slope $\sigma = 1/2\lim_{\omega\to 0}\chi^{\perp}(\omega,0)/\omega$. The second will be solutions with lightlike spatial momentum in which we will be able to calculate the photoproduction rate.

To perform the study we will numerically integrate equation (4.6) from the singular shell to the boundary. As mentioned in the previous section, we will use a regularising index $\eta_0^{(*)} = 0$, so that the function $\mathcal{A}_{\perp}(u)$ is regular at the singular shell. Once the numerical solution is obtained we read the asymptotic behavior near the boundary and from that data we extract the coefficients $\mathcal{B}_m$, which will depend on all the parameters considered.

5.1 Transverse fluctuations at zero momentum

Setting $\mathfrak{q} = 0$ allows us to plot the spectral function as a function of $\mathfrak{w}$ and examine the evolution of it across the parameter space spanned by $(e, \tilde{n}_q, m_q)$. A fairly important change in shape is observed upon crossing the conical embedding transition region in the (m_q, e) plane (see figure 6). In figure 14 we show an example sequence of spectral functions for a range of values of e and with $\tilde{n}_q = 0.012$ and $m_q = 3.5$. Over a very small range, $3.4 \lesssim e \lesssim 3.7$, the magnitude of the spectral function drops by around two orders of magnitude and the sharp peaks disappear completely, leaving a smooth profile with very wide oscillations which can no longer be interpreted as quasiparticles. This rapid crossover in behavior is a relic of the very fast change in behavior of the embedding in a small region of the (m_q, e) parameter space.

A physical observable related to the spectral function at zero momentum is the conductivity. A perfect agreement between our numerical computation of this quantity and that performed analytically, eq. (4.15), is found

$$\tilde{\sigma} = \frac{1}{2}\lim_{\mathfrak{w}\to 0}\frac{\tilde{\chi}^{\perp}}{\mathfrak{w}} = \sqrt{\sqrt{1+e^2}\,(1-\psi_\star^2)^3 + \frac{\tilde{n}_q^2}{1+e^2}}\,. \tag{5.5}$$

5.2 Lightlike momentum and photoproduction

Here we generalise the previous calculation to the case of lightlike momenta. This allows us to study photoproduction and discover how an electric field affects the brightness of the plasma [29, 31].

The emission rate for real photons is controlled by the spectral function evaluated at lightlike momenta $\omega = |\mathbf{k}|$. Given that on the light cone $\Pi_{||} = 0$ (otherwise we would have a divergence in the retarded Green's function), we can express the emission rate entirely in terms of $\Pi_{\perp}$ as follows

$$d\Gamma_{\gamma} = -\frac{d\mathbf{k}^3}{(\pi)^3}\frac{e_{\mathrm{EM}}^2}{2|\mathbf{k}|}\frac{\mathrm{Im}\,\Pi_{\perp}(k^{\mu})}{e^{\omega/T}-1}\bigg|_{\omega=|\mathbf{k}|}\,, \tag{5.6}$$

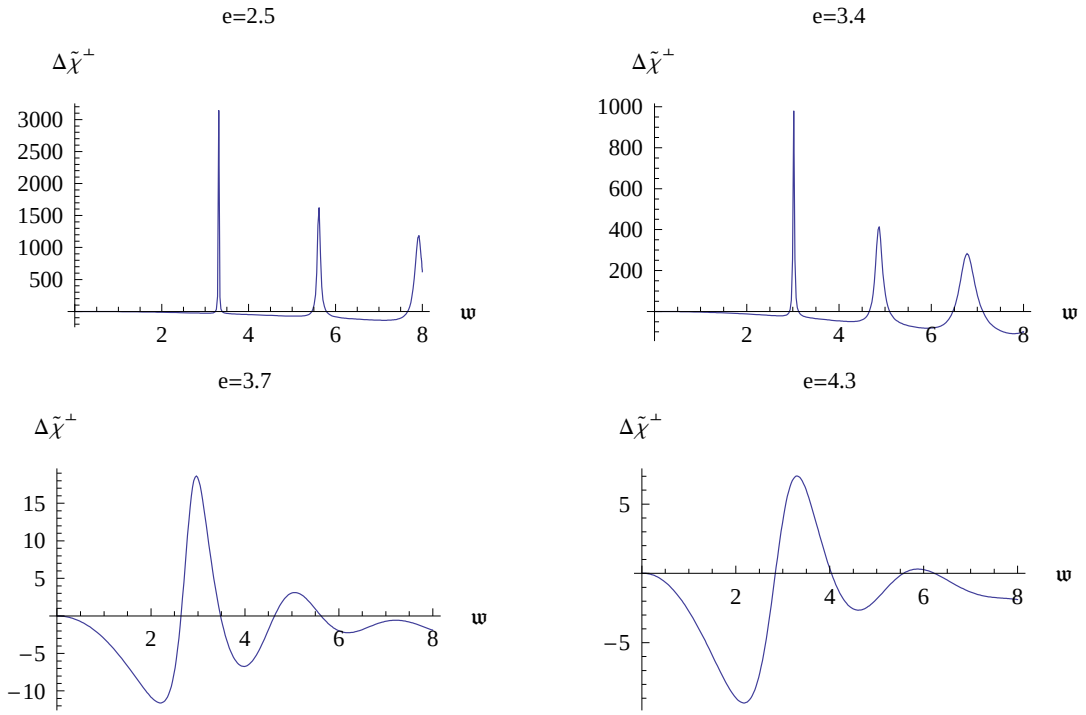

Figure 14. The difference, $\Delta\tilde{\chi}^{\perp}$, between the spectral function $\tilde{\chi}^{\perp}(\mathfrak{w})$ and the zero temperature limit with increasing values of the electric field e at fixed value of the baryon density ($\tilde{n}_q = 0.012$) and mass ($m_q = 3.5$). After crossing the line of conical embeddings the peaks broaden very quickly into wide oscillations which cannot be interpreted as quasiparticles.

where $e_{\rm EM}$ is the electromagnetic coupling constant. Since our system lacks isotropy, strictly speaking, the above expression only applies to photons with $k^\mu = \omega(1,0,0,1)$ which propagate parallel to the electric field $\vec{E} = (0,0,E_z)$[9]. In figure 15 we see a series of curves that represent the value of $d\Gamma(\mathfrak{w})/d\mathfrak{w}$ normalized by $(2\pi T)e_{\rm EM}^2/\pi^2$. The Boltzman factor means that the relevant structure can only be seen in the range of frequencies $\mathfrak{w} \in (0,2)$. The curves are plotted for $m_q = 3$ and increasing values of the electric field $e = 2.3, 2.5, 2.7$ and 3. A strong enhancement is observed upon traversing the crossover region.

The rates are similar and exhibit a peak at $\mathfrak{w} \sim 0.25$. We could choose this as a representative value of the overall magnitude of the photoproduction, and see how it changes as we move across the (m_q, e) space. Alternatively we can integrate (5.6) in $\omega \in (0,\infty)$, which gives the total number density of thermal photons emitted parallel to the electric field (per unit momentum space solid angle). The result can be seen in figure 16. A remarkable similarity with the plots in figure 12 is observed. Of course a knowledge of the differential photoproduction rate for $\vec{q}$ not parallel to $\vec{E}$ would be extremely interesting. We leave this analysis for a further study.

[9]we would like to thank David Mateos for pointing out this subtlety

JHEP09(2009)032

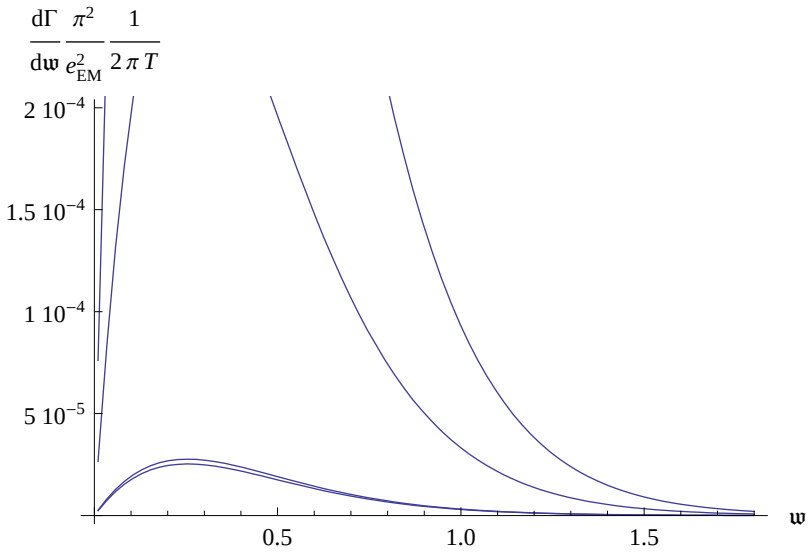

Figure 15. Photoproduction density rate in the direction of the electric field, from low to high, at values of $e = 2.3$, 2.5, 2.7 and 3 with $\tilde{n}_q = 0.05$.

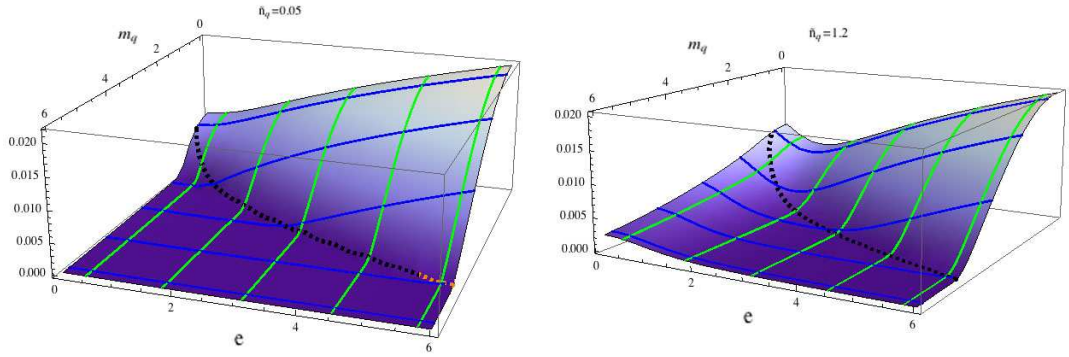

Figure 16. Integrated photoproduction $(2\pi)^3\Gamma/e^2_{\rm EM}$ as a function of (m_q, e).

6 Discussion and conclusions

In this paper we have studied in detail the effect of an external electric field on the physical properties of a large N_c finite temperature Yang Mills plasma with a single flavour in the quenched approximation. In addition to the strength of the electric field the free parameters of our model have been the baryon density and the quark mass and we have explored this three-dimensional parameter space thoroughly. The singular shell which is a direct consequence of a large enough ratio of the electric field strength to the quark mass appears to play a key role in the quantities of the gauge theory living on the AdS boundary. Although the singular shell does not have the geometrical properties to label it a horizon, in many ways its effects appear to be similar to those of a real black hole horizon. In particular the attractor-like behavior whereby the solution of the embedding is

JHEP09(2009)032

fixed uniquely by a single boundary condition constrains the solutions greatly. Continuing the embedding inside the singular shell gives us solutions which may or may not have a conical singularity, depending on the values of e and m_q for a particular value of $\tilde{n}_q$. Indeed this conical singularity appears and then disappears as we traverse the (e, m_q) parameter space. The region in which this transition happens appears to play a key role as a crossover region in the behavior of many physical quantities. However, it may be interpreted that this region of conical singularities is only a symptom of what is happening at the singular shell.

In [19] it was argued that the size of the effective horizon induced on a probe $D7$-brane greatly affected the spectral function, with a small induced horizon leading to a series of sharp peaks in the spectral function and long-lived quasiparticles, whereas a large effective horizon led to a smooth spectral function and the disappearance of the quasiparticle interpretation as the poles in the quasinormal mode spectrum disappeared into the complex frequency plane. This phenomenology is related to the fact that the incoming wave boundary conditions at the horizon allow the absorption of energy into the system more rapidly if the effective horizon is larger. Quasiparticles have shorter lifetimes if, in the holographic picture, their energy can be dissipated into a larger effective horizon.

Although the interpretation of the singular shell as any sort of effective horizon is unclear, we do appear to have a very similar phenomenology in the work presented here. For a large induced singular shell area on the $D7$-brane (corresponding to a small value of $\psi_\star$) the spectral function is smooth, while for a small induced singular shell area, the spectral function is sharply peaked. The crossover region is then traced to a small region in parameter space where the area of the induced singular shell changes very quickly from a small value to a large value, allowing, for instance, for several orders of magnitude change in the photoproduction rate.

One may ask if this is not due to the effective horizon itself, however it appears that this is not so. As we pass through the cross-over region, the size of the effective horizon does not increase monotonically, whereas it seems that the widths of the peaks in the spectral function, for example, do. If the widths of peaks in the spectral function were determined by the size of the effective horizon as in [19] one should see the same monotonic behaviour. For this reason it appears that the important IR quantity is the area of the effective singular shell, where again the incoming wave boundary conditions which completely fix the UV behaviour, seem to have a similar effect to the horizon in the $e = 0$ case. In addition, because of the attractor-like mechanism at the singular shell, effectively the behavior outside the singular shell is completely shielded from what is happening inside. Any additional force that one applied to the brane inside the singular shell will not be felt outside. It is however true that the changes at the singular shell are reflected both in the UV physics and the behavior of the brane within the singular shell. For this reason the line of conical embeddings simply appears to be a good marker of the region where we have discovered such interesting effects.

It should be noted that the calculation for the susceptibility, eq (3.11), does appear to rely on the behavior inside the singular shell. This is because we have imposed the vanishing of the time component of the gauge field on the horizon. A check that the susceptibility does not in fact depend on the region inside the singular shell would be to calculate it via

JHEP09(2009)032

the Einstein relation for which we would need to calculate the diffusion constant from the longitudinal correlator. We leave this investigation for the future.

There may be hints to the physics behind the crossover region coming from the analytic expression from the conductivity. Indeed we can see that there are two terms in this expression, one of which is clearly related to the size of the induced singular shell area and increases with increasing electric field strength, while the other decreases with the electric field strength. As you increase e or $1-\psi_\star^2$ the dominant term in the conductivity will change from one to the other. Because m_q and not $\psi_\star$ is the more physical parameter in our gauge theory the contribution of the first term is less clear when we plot physical quantities as a function of m_q. We conjecture that the two competing effects which are very clear in the expression for the conductivity (namely pair-production and free charges respectively) may explain the rapid change in behavior across the crossover region. It would certainly be interesting to investigate the interplay between the two competing effects in more depth.

The stability of the solutions in the crossover region is a subtle issue. We have been able to show that for a region of the parameter space there exist unstable solutions, which are seen with a multivaluedness in $m_q(\psi_\star)$ and therefore a first order phase transition. These appear, for large enough electric field, to lie within a region of conical embedding solutions. A full stability analysis is beyond the scope of this paper and it will be very interesting to see if the whole region of parameter space which includes the conical solutions is in fact unstable. This will be seen through a thorough thermodynamic analysis and a study of the existence of tachyonic quasinormal modes on the classical embedding. We leave this analysis for future study.

It would be extremely exciting if one could test these predictions of a fast crossover/phase transition region in the laboratory. However, it appears that the current technical limitations in heavy-ion experiments do not allow for the investigation of the quark gluon plasma in the presence of external electric fields. What may be more practical would be a condensed matter system modeled holographically, and demonstrating a similar phenomenology to the one studied in this paper. An obvious example would be the defect $D3/D5$ system.

Acknowledgments

We would like to express our gratitude to Daniel Arean, Andy O'Bannon, Veselin Filev, David Mateos, Rene Meyer, Alfonso Ramallo and Dimitrios Zoakos. This work was supported in part by by the MICINN and FEDER (grant FPA2008-01838), by the Spanish Consolider-Ingenio 2010 Programme CPAN (CSD2007-00042), by Xunta de Galicia (Conselleria de Educacion and grant PGIDIT06 PXIB206185PR). J.T. and J.S. have been supported by MICINN of Spain under a grant of the FPU program and by the Juan de la Cierva program respectively.

References

[1] A. Karch and A. O'Bannon, *Metallic AdS/CFT*, *JHEP* **09** (2007) 024 [arXiv:0705.3870] [SPIRES].

JHEP09(2009)032

[2] D.T. Son, *Toward an AdS/cold atoms correspondence: a geometric realization of the Schrödinger symmetry*, *Phys. Rev.* **D 78** (2008) 046003 [arXiv:0804.3972] [SPIRES].

[3] M. Ammon, J. Erdmenger, M. Kaminski and P. Kerner, *Flavor superconductivity from gauge/gravity duality*, arXiv:0903.1864 [SPIRES].

[4] S.A. Hartnoll, *Lectures on holographic methods for condensed matter physics*, arXiv:0903.3246 [SPIRES].

[5] V.G. Filev, C.V. Johnson, R.C. Rashkov and K.S. Viswanathan, *Flavoured large-N gauge theory in an external magnetic field*, *JHEP* **10** (2007) 019 [hep-th/0701001] [SPIRES].

[6] V.G. Filev, *Criticality, scaling and chiral symmetry breaking in external magnetic field*, *JHEP* **04** (2008) 088 [arXiv:0706.3811] [SPIRES].

[7] T. Albash, V.G. Filev, C.V. Johnson and A. Kundu, *Finite temperature large-N gauge theory with quarks in an external magnetic field*, *JHEP* **07** (2008) 080 [arXiv:0709.1547] [SPIRES].

[8] J. Erdmenger, R. Meyer and J.P. Shock, *AdS/CFT with flavour in electric and magnetic Kalb-Ramond fields*, *JHEP* **12** (2007) 091 [arXiv:0709.1551] [SPIRES].

[9] T. Albash, V.G. Filev, C.V. Johnson and A. Kundu, *Quarks in an external electric field in finite temperature large-N gauge theory*, *JHEP* **08** (2008) 092 [arXiv:0709.1554] [SPIRES].

[10] V.G. Filev, C.V. Johnson and J.P. Shock, *Universal holographic chiral dynamics in an external magnetic field*, arXiv:0903.5345 [SPIRES].

[11] O. Bergman, G. Lifschytz and M. Lippert, *Response of holographic QCD to electric and magnetic fields*, *JHEP* **05** (2008) 007 [arXiv:0802.3720] [SPIRES].

[12] O. Bergman, G. Lifschytz and M. Lippert, *Magnetic properties of dense holographic QCD*, *Phys. Rev.* **D 79** (2009) 105024 [arXiv:0806.0366] [SPIRES].

[13] K.-Y. Kim, S.-J. Sin and I. Zahed, *Dense and hot holographic QCD: finite baryonic E field*, *JHEP* **07** (2008) 096 [arXiv:0803.0318] [SPIRES].

[14] A. Karch and E. Katz, *Adding flavor to AdS/CFT*, *JHEP* **06** (2002) 043 [hep-th/0205236] [SPIRES].

[15] J. Erdmenger, N. Evans, I. Kirsch and E. Threlfall, *Mesons in gauge/gravity duals — A review*, *Eur. Phys. J.* **A 35** (2008) 81 [arXiv:0711.4467] [SPIRES].

[16] S. Nakamura, Y. Seo, S.-J. Sin and K.P. Yogendran, *A new phase at finite quark density from AdS/CFT*, *J. Korean Phys. Soc.* **52** (2008) 1734 [hep-th/0611021] [SPIRES].

[17] S. Kobayashi, D. Mateos, S. Matsuura, R.C. Myers and R.M. Thomson, *Holographic phase transitions at finite baryon density*, *JHEP* **02** (2007) 016 [hep-th/0611099] [SPIRES].

[18] R.C. Myers and A. Sinha, *The fast life of holographic mesons*, *JHEP* **06** (2008) 052 [arXiv:0804.2168] [SPIRES].

[19] J. Mas, J.P. Shock, J. Tarrio and D. Zoakos, *Holographic spectral functions at finite baryon density*, *JHEP* **09** (2008) 009 [arXiv:0805.2601] [SPIRES].

[20] M. Kaminski, K. Landsteiner, J. Mas, J.P. Shock and J. Tarrio, work in progress.

[21] A. O'Bannon, *Hall conductivity of flavor fields from AdS/CFT*, *Phys. Rev.* **D 76** (2007) 086007 [arXiv:0708.1994] [SPIRES].

[22] J. Erdmenger, N. Evans, I. Kirsch and E. Threlfall, *Mesons in gauge/gravity duals — A review*, *Eur. Phys. J.* **A 35** (2008) 81 [arXiv:0711.4467] [SPIRES].

JHEP09(2009)032

[23] C.P. Herzog, A. Karch, P. Kovtun, C. Kozcaz and L.G. Yaffe, *Energy loss of a heavy quark moving through $N = 4$ supersymmetric Yang-Mills plasma*, *JHEP* **07** (2006) 013 [hep-th/0605158] [SPIRES].

[24] S.S. Gubser, *Momentum fluctuations of heavy quarks in the gauge-string duality*, *Nucl. Phys.* **B 790** (2008) 175 [hep-th/0612143] [SPIRES].

[25] J. Casalderrey-Solana and D. Teaney, *Transverse momentum broadening of a fast quark in a $N = 4$ Yang-Mills plasma*, *JHEP* **04** (2007) 039 [hep-th/0701123] [SPIRES].

[26] D. Mateos, R.C. Myers and R.M. Thomson, *Thermodynamics of the brane*, *JHEP* **05** (2007) 067 [hep-th/0701132] [SPIRES].

[27] J. Mas, J.P. Shock and J. Tarrio, *A note on conductivity and charge diffusion in holographic flavour systems*, *JHEP* **01** (2009) 025 [arXiv:0811.1750] [SPIRES].

[28] J. Erdmenger, M. Kaminski and F. Rust, *Holographic vector mesons from spectral functions at finite baryon or isospin density*, *Phys. Rev.* **D 77** (2008) 046005 [arXiv:0710.0334] [SPIRES].

[29] S. Caron-Huot, P. Kovtun, G.D. Moore, A. Starinets and L.G. Yaffe, *Photon and dilepton production in supersymmetric Yang-Mills plasma*, *JHEP* **12** (2006) 015 [hep-th/0607237] [SPIRES].

[30] D.T. Son and A.O. Starinets, *Minkowski-space correlators in AdS/CFT correspondence: recipe and applications*, *JHEP* **09** (2002) 042 [hep-th/0205051] [SPIRES].

[31] D. Mateos and L. Patino, *Bright branes for strongly coupled plasmas*, *JHEP* **11** (2007) 025 [arXiv:0709.2168] [SPIRES].

JHEP09(2009)032